Title

Unimicellar hyperstars as multi-antigen cancer nanovaccines displaying clustered epitopes of immunostimulating peptides

Journal

Biomaterials Science, 6(11)

ISSN

2047-4830

Authors

Kakwere, Hamilton
Ingham, Elizabeth S
Allen, Riley
et al.

Publication Date

2018-11-01

DOI

10.1039/c8bm00891d

Peer reviewed

HHS Public Access

Author manuscript

Biomater Sci. Author manuscript; available in PMC 2019 November 01.

Published in final edited form as:

Biomater Sci. 2018 November 01; 6(11): 2850–2858. doi:10.1039/c8bm00891d.

Unimicellar hyperstars as multi-antigen cancer nanovaccines displaying clustered epitopes of immunostimulating peptides†

Hamilton Kakwere[a,b], **Elizabeth S. Ingham**[a], **Riley Allen**[a], **Lisa M. Mahakian**[a], **Sarah M. Tam**[a], **Hua Zhang**[a,b], **Matthew T. Silvestrini**[a], **Jamal S. Lewis**[a], and **Katherine W. Ferrara**[b,*]

[a]Department of Biomedical Engineering, University of California (Davis), Davis, CA 95616, USA

[b]Molecular Imaging Program at Stanford (MIPS), Department of Radiology, Stanford University, Stanford, CA 94305, USA

Abstract

Unimicellar hyperstar macromolecular chimeras displaying multiple melanoma peptide antigens were prepared primarily *via* a combination of click chemistry and esterification reactions starting from a biodegradable hyperbranched polymer template. Solubilization of the hyperstars in aqueous solution afforded a multi-antigen unimicellar cancer nanovaccine of about 20 nm. The nanovaccine showed good biocompatibility and uptake by dendritic cells *in vitro*. An *in vivo* evaluation of the nanovaccine therapeutic efficacy against melanoma in mice implanted with B16OVA tumors revealed significantly greater T-cell recruitment and improved survival rates for mice treated with nanovaccine and adjuvant compared to non-treated mice.

Graphical Abstract

Multi-antigen bearing biodegradable unimicellar nanovaccines based on hyperstar macromolecular chimeras for cancer therapy.

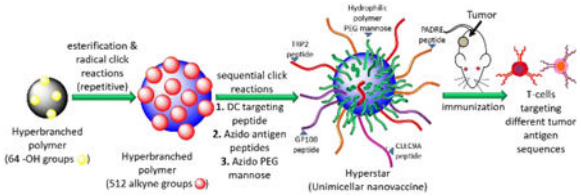

The design of peptide-based nanovaccines for cancer immunotherapy has received growing attention in recent years.[1–4] This is driven by the need to overcome the shortcomings of peptide vaccines such as low immunogenicity, poor drainage to lymph nodes and

†Electronic supplementary information (ESI) available:

*Correspondence: kwferrara@ucdavis.edu/ kwferrar@stanford.edu.

Ethical statement

All animal experiments were performed under a protocol approved by the Institutional Animal Care and Use Committee (IACUC) of the University of California, Davis. Experiments were performed in compliance with relevant laws or guidelines and followed institutional guidelines. The IACUC at UC Davis is accredited by the Association for Assessment and Accreditation of Laboratory Animal Care International (AAALAC) and has been accredited since 1966.

Conflicts of interest

There are no conflicts to declare.

tolerogenicity.[5] Moreover, the presentation of peptide antigen vaccines on the surface of nanoparticles gives rise to a clustering effect (multivalent antigen display) which has been advocated to lead to improved efficacy.[6, 7] Recent technological advances in cancer immunotherapy indicate that effective and specific immune responses can be generated from mutated sequences of tumor-associated peptide antigens (neoantigens), thus the sustained need for innovative strategies to fabricate nanovaccines targeted for the clinic has been revitalized.[8, 9] For clinical development, the ease of preparation, commercial availability of reagents, upscaling, cost, versatility, size, toxicity, and robustness are among the key considerations of the design and fabrication of these nanomaterials.[10]

The fabrication of nanovaccines for immunotherapy based on neoantigen identification is further made challenging by the large number of potential immunostimulating peptide sequences generated during their identification.[11] Thankfully, the use of multi-antigen peptide vaccines that combine multiple immunostimulating epitopes in one long sequence or as a formulation of a pool of antigen peptides is a favoured strategy for inducing a strong immune response through recruitment of broadly cross-reactive T-cells capable of targeting multiple tumor antigens.[12, 13] However, the need for their incorporation into nanoparticles is retained to avoid the aforementioned problems related with administration of free peptide antigens. Accordingly, nanocarriers designed for delivery of the antigens need to have a large number of surface functional groups available to accommodate the attachment of a significant number of different peptide epitopes. Attachment of the antigens to the surface of metal nanoparticles is a possible strategy due to their large surface area and ease of synthesis.[14] However, there are long-term toxicity and biodegradability concerns with some metals, in addition to the possibility of inflammation and lack of versatility in terms of functional groups that can be used.[15, 16] Self-assembled nanostructures such as block copolymer micelles and lipids also present large surface areas with reactive groups on the surface but suffer from dissociation below critical micelle concentration which leads to poor circulation and rapid clearance.[17] Unimicellar nanostructures based on amphiphilic dendrimers, hyperbranched polymers, and cross-linked block copolymer micelles present a viable alternative as they do not suffer from disaggregation upon dilution and are more robust towards shearing during circulation *in vivo*.[18, 19] Among the unimicellar nanostructures, amphiphilic hyperbranched polymers are attractive from a synthetic viewpoint, with the potential for upscaling and the commercial availability of easily modifiable hyperbranched polymer cores (templates) at modest prices.[20, 21]

We have recently reported the preparation of nanovaccines based on a hyperbranched polymer (Boltorn H40). Boltorn H40 is advantageous in that it is both commercially available and has limited toxicity.[22] The reported approach is high-yielding, circumvents the use of potentially toxic copper metal and the high selectivity of the strain promoted azide-alkyne click (SPAAC) reaction makes it tolerant to a wide range of peptide chain functionalities. However, a limitation with commercially available branched polymers is that the number of sites available for conjugation of antigens is restricted by whatever the supplier makes. This limitation rarely rivals what's achieved with block-copolymer micelles which tend to have aggregation numbers in the order of several hundred.[23] Indeed, in our previous work, we observed the number of sites available for attaching antigens per branched molecule was ca. 37 against the reported theoretical number of 64. Taking into

account the need to avoid peptide antigen entanglement,[24] the maximum number of antigens attached to the surface was limited to 10% of available sites implying only ca.4 antigens were available per branched molecule. Such a low loading is not ideal for the fabrication of a multi-antigen peptide nanovaccine. In an effort to produce multi-antigen bearing nanovaccines with high conjugation capacity, stability upon dilution or *in vivo* circulation, we demonstrate a facile strategy to obtain unimicellar hyperstar macromolecular chimeras with multivalent display of diverse immunostimulating peptide antigens. Our generic approach takes advantage of commercially available non-toxic branched polymers to prepare nanovaccines with high conjugation capacity akin to block copolymer micelles. Using Boltorn H40 as a template, we show that the size of the lipophilic core and conjugation capacity can be easily expanded from 64 to 512 (theoretical) virtually *via* the combination of highly efficient esterification and metal-free click reactions with facile product recovery procedures between the steps (Figure 1).[25] Furthermore, apart from the peptide antigens (which are prepared using an automated process), the strategy employs commercially available reagents thus minimizing the required synthetic effort. Subsequent sequential strain promoted azide-alkyne click (SPAAC)[26] conjugation of peptides (CLEC9A (dendritic cell targeting),[27] GP100 (melanoma antigen), TRP2 (melanoma antigen),[28] PADRE (T-helper peptide))[29] and hydrophilic polymer conjugation afforded core-shell like amphiphilic hyperstar[18] macromolecular chimeras with sizes of ca. 20 nm, which is ideal for nanovaccines.[30, 31] We also demonstrate the potential application of our nanovaccines *in vivo* against a B16OVA melanoma tumor model.

Our strategy for the generation of the nanovaccines is outlined in Figure 1. We employed Boltorn H40, a biodegradable polyester with 64 (theoretical) reactive end groups (hydroxyl), as a scaffold for the generation of a hyperbranched polymer with 512 (theoretical) reactive sites to afford an azide reactive polymer with increased conjugation capacity that rivals that of block copolymer micelles. Initially, (**1**) was prepared by converting 5-hexynoic acid to the more reactive acid chloride using oxalyl chloride and obtained in quantitative yield. Successful formation of (**1**) was confirmed by FTIR (ESI, Fig. S1). BoltornH40 was alkyne functionalized by coupling with (**1**) and the functionality of the resultant polymer was expanded to 128 sites (theoretical) *via* the high yielding thiol-yne click reaction with (**2**).[25] The isolated product exhibited good solubility in THF and it was alkyne functionalized by reaction with an acid chloride (**1**). Through the repetition of the efficient thiol-yne and acid chloride esterification reactions, the hyperbranched polymer size and end group functionality were increased. The final thiol-yne reaction being done using (**3**) instead of (**2**) to obtain an amine reactive polymer that was subsequently coupled with (**4**). Importantly, our approach ensured the presence of ester and amide groups during the expansion to retain biodegradability of the material which is favorable for nanomaterials aimed at *in vivo* applications. Remarkably, product recovery at each step was achieved in a facile manner *via* precipitation in non-solubilizing solvents. Success of the reactions was ascertained by ^{1}H NMR, size exclusion chromatography (SEC) (Figure 2) and FTIR (ESI, Fig. S2). The ^{1}H NMR spectra in Figure 2 show resonances consistent with the formation of the desired products from the polymer with 128 reactive sites to the alkyne polymer with 512 reactive sites. Moreover, SEC showed an increase in molecular weight following each reaction step evidenced by the decreasing retention time, with broad peaks typical of hyperbranched

polymers. Following each esterification reaction, the broad -OH stretch peak due the terminal hydroxyl groups of the starting hyperbranched polymer disappeared whilst the peak due to the alkyne-C≡C-H stretch appeared as observed by FTIR (ESI, Fig. S2). On the other hand, the radical reaction between the alkyne groups with **2** or **3** resulted in the broad–OH stretch peak (**2**) or the broad–COOH stretch (**4**) being observed upon analysis of the purified products by FTIR (ESI, Fig. S2). A prolonged reaction between known amounts of the cyclooctyne-terminated hyperbranched polymer with phenyl 6-azidohexanoate enabled the empirical determination of the number of available alkynes as 296 alkynes/molecule based on consumption of the azide and the loading as ca. 1.4 μmol/mg.[22]

To demonstrate the preparation of a multi-peptide epitope displaying nanovaccine, attachment of melanoma peptide antigens (GP100 and TRP2) and a T-helper cell peptide (PADRE) was implemented (Figure 1). The availability of a large number of conjugation sites also allows for inclusion of targeting peptides, for instance the targeting of dendritic cells (DCs) which play a key role in the initiation of adaptive immune responses through antigen presentation. Thus, we also included a CLEC9A+ DC targeting peptide (CLEC9A) to demonstrate the versatility of our strategy.[27, 32] Targeting antigen carrying nanoparticles to DCs can lead to increased uptake which potentiates the generation of an immunogenic response.[27] Fmoc solid phase peptide synthesis (SPPS) strategy was utilized to prepare azide-bearing analogues of the peptides that could be coupled with the hyperbranched polymer (Figure 2, A–B) using metal-free click chemistry which obviates toxicity while providing high yields and tolerance to a wide range of functional groups (see ESI Fig. S3–S6 for peptide structures, LC-MS and MALDI-TOF results). Initially, the CLEC9A peptide (0.75 mol% of available alkynes) was reacted with the hyperbranched alkyne, which after 24 hours was observed to have been completely consumed based on HPLC (Figure 2C). The remaining peptides were subsequently added, one at a time, to the branched polymer (10 mol% of available alkynes each) without any isolation between the additions, while allowing a 24-hour reaction period following each addition. The remaining peptides were also completely consumed by the alkyne polymer as assessed by HPLC (Figure 2C). Based on the HPLC results which show complete consumption of the peptides, the conversion (hence incorporation) is therefore 100%. It is noteworthy that we were also able to achieve the same outcome by adding the combined peptides at the same time (after attaching the CLEC9A peptide) but more reaction time was required to observe complete consumption based on HPLC (at least 72 hours). Interaction of the peptides with the SEC column prevented elution and therefore our determination of change in molecular weight. Lastly, the amphiphilic structure was obtained by coupling PEG mannose to the remaining available alkynes by addition of an excess of the PEG_{12} mannose (300 mol%) to the peptide-functionalized branched polymer. Incorporation of PEG_{12} mannose was confirmed through ^{1}H NMR after the removal of excess free polymer by dialysis (ESI, Fig. S7). The amino acid composition and content was confirmed by amino acid analysis (ESI, Table S1). The amino acid analysis is based on PADRE, GP100 and TRP2 peptides (as one long sequence) since the amount of the CLEC9A peptide is negligible (only 0.75 mol% of starting alkyne). Interestingly, when analysis of the hyperstar macromolecular chimeras was conducted utilizing SEC, the material was eluted indicating a change in chemical character of the corona as compared to the peptide-decorated particle. Only a subtle shift in molar mass compared to the

hyperbranched alkyne polymer before peptide/polymer coupling was observed by SEC possibly due to the influence of peptide interaction with the column or small change in hydrodynamic volume due to compactness of the structure of the hyperstars (ESI, Fig. S8).

Aqueous solubilization of the prepared material was achieved via dialysis from an organic solvent (DMF)-water solution to afford the nanovaccines. For nanovaccines, sizes in the range 10 – 50 nm are ideal. By dynamic light scattering (DLS), the nanoparticles obtained were observed to have an average diameter of 21 ± 4 nm and a zeta potential of −7 ± 0.5 mV (Figure 3A left). Observation of the nanoparticle morphology by TEM revealed the presence of mostly spherical and elliptical-shaped nanoparticles with a calculated average diameter of 21 ± 4 nm (major axis considered for ellipse like particles) (Figure 3A right). The amount of peptide realized after purification was 10–15% (w/w). An assessment of the toxicity of the nanovaccines and constituent peptides was conducted *via* an MTT assay (Figure 3B). Ideally, the antigen carrier should be non-toxic, and thus a material decorated with PEG mannose only (no peptides) was prepared and its toxicity was also evaluated. The polymer-only nanoparticles and the peptide conjugated nanoparticles were negligibly toxic up to 1 mg/mL over a 48-hour period. Among the peptides, the GP100 peptide was non-toxic up to 0.5 mg/mL whereas the PADRE peptide showed some toxicity similar to that observed for TRP2 in our previous study.[22] As in the case of TRP2, the toxicity observed for PADRE is linked to the hydrophobicity of the peptide which likely causes cell membrane destabilization. Nevertheless, the results show that the toxicity of the peptides was reduced by merging them with the polymer and their inclusion into the nanoparticles. Cell viability studies were also conducted against Raw 264.7 macrophages (antigen presenting cells) and the results are shown in ESI, Fig. S9. The peptide-conjugated nanoparticles show good biocompatibility with negligible toxicity being observed below 0.5 g/L and greater than 80% viability at the highest concentration of 1 g/L. The cell viability was above 80% for most of the free peptides (except TRP2) below 0.25 g/L while at the highest concentration viability was reduced to about 60%. For TRP2, viability was 50%−60% within the concentration range of the study (0.05–0.5 g/L). The results suggest that the Raw 264.7 macrophages cell line is generally more sensitive to the materials used in this study (especially at high concentration) compared to the cancer cells (B16-F10). However, the material of primary interest (peptide-conjugated nanoparticles) exhibited low toxicity towards the Raw 264.7 macrophages. It is noteworthy that the amount of material injected for vaccination in vivo is typically ca. 300 μg which translates to a low concentration where both the peptides and the peptide-conjugated nanoparticles show high cell viability and hence biocompatibility. For instance, using a typical mouse weight of 20 grams, the concentration will be 0.0015 mg/gram or if all of the material ends up in the blood, the concentration will be 0.2 mg/mL (1.5 mL blood volume/mouse).[22]

Next, the uptake of the nanoparticles by DCs (murine bone marrow derived DCs) in vitro was studied. Fluorescent equivalents of the hyperstars were prepared using the sequential SPAAC approach discussed above. Azido-PEG_3−fluorescein (10 mol%) (ESI, Fig. S10) was first coupled to the BH40-DBCO512, followed by addition of CLEAC9A, the remaining peptides and PEG_{12}−mannose as previously discussed herein. Complete consumption of the dye was observed by HPLC, and the sample was also purified by dialysis and centrifugal filtration removing any traces of free dye and polymer. For preparation of the polymeric

particles (no-peptide), excess PEG_{12}−mannose was added after conjugation of the fluorescent label. Aqueous solubilization of the conjugates gave fluorescent nanoparticles with a diameter of ca. 22 nm and a zeta potential of −8 mV (ESI, Fig. S11). Generally, an increase in nanoparticle uptake with time was observed over a 24-hour period as assayed by flow cytometry (Figure 3C). Peptide-conjugated nanoparticles were taken up more than fluorescently-labelled Polymer NPs particles suggesting that the presence of the peptides increased uptake probably due to the hydrophobicity of the TRP2 and PADRE peptides which favors interaction with the cell membrane.[22] A decrease in fluorescence intensity was observed for the peptide-conjugated nanoparticles at 24 hours compared to 4 hours. This is likely due to saturation of the receptor-mediated binding and internalization of the peptide-conjugated nanoparticles which took place during the early stages of incubation leading to reduced uptake efficiency over time. As the endocytosed fluorescently-labelled nanoparticles are degraded in lysosomes, coupled with diminished uptake, fluorescence is reduced. On the other hand, for the polymer nanoparticles, the total internalization is substantially (more than 10-fold) lower but there is a gradual uptake of nanoparticles over time. Another possibility is that the amount of the uptaken peptide NPs led to concentration quenching. Visual confirmation of nanoparticle uptake was obtained through confocal microscopy. The DCs were stained with LysoTracker Red (acidic compartments) and 4′,6-diamidino-2-phenylindole (DAPI)(nuclei) for co-localization assay and identification of intracellular distribution via confocal microscopy. Indeed, co-localization of the nanoparticles with LysoTracker Red is observed (green spots) after incubation of the nanoparticles with cells for 4 hours (Fig. 3D and Fig. S12) The particles appear to be localized in endosomes distributed within the cytoplasm and around the nuclei.

The *in vivo* application of the nanovaccines for the treatment of melanoma was first studied by looking at the immune response elicited in mice upon vaccination with nanovaccine plus adjuvant (Peptide NPs+CpG), adjuvant alone (CpG) or saline (NTC). Mice implanted with B16OVA cells were vaccinated following the protocol shown in Figure 4A and sacrificed 14 days after cell implant to collect organs for the detection of immune cell populations employing flow cytometry. Analysis of the harvested tumors indicates mice treated with the Peptide NPs+CpG had the lowest number of remaining live cells, indicating smaller size tumors compared to the CpG-only and NTC groups (Figure 4B). Treatment cohorts displaying the lowest number of viable tumor cells, also had correspondingly higher frequencies of tumor infiltrating T-cells (Figure 4C), implicating T-cells as key players in the eradication of tumor cells. The population of cytotoxic $CD8^+$ T-cells in the Peptide NPs +CpG cohort was significantly greater than that for the NTC group while no significant difference was observed between the NTC and adjuvant groups (Figure 4D). An increased number of cells in the lymph nodes (Figure 4E) and spleen (ESI, Fig. S13) was observed for the CpG and Peptide NPs+CpG groups. The cell count in both the lymph nodes and spleen for the Peptide NPs+CpG groups was significantly greater than the NTC cohort while no significant difference was observed between the CpG and NTC groups in the lymph nodes. In the spleen, a significant difference was observed for both the CpG ($p \leq 0.05$) and Peptide NPs+CpG ($p \leq 0.01$) groups versus the NTC group albeit the cell count for the Peptide NPs +CpG group was greater than that of the CpG group (ESI, Fig. S13). Enlargement of lymph nodes and spleen is typically consistent with immune system activation. The overall number

of leukocytes (including T-cells) in the lymph nodes was also significantly greater for the Peptide NPs+CpG group than the NTC group with no significant difference observed between the CpG-only and NTC groups (Figure 4F–G). Although the T-cell population appears to be reduced in the spleen (ESI, Fig. S13), the absolute number of T-cells is increased due to the enlargement of the spleen (hence total cell count) for the CpG-only and Peptide NPs+CpG groups (data not shown). An increase in DC frequency in the lymph node, spleen and blood was also observed for the CpG and Peptide NPs+CpG groups (data not shown), which is suggestive of an enhanced innate immune response in these treatment cohorts. Overall, the results suggest that the combination of nanovaccine with adjuvant elicits a notable immune response and, most importantly, significantly enhances cytotoxic $CD8^+$ T-cells responsible for tumor cell destruction and subsequent inhibition of tumor growth.

Finally, the therapeutic potency of the nanovaccines was assessed through a survival study of C57BL/6 mice implanted with B16OVA tumors. The two-treatment protocol followed on days 3 and 10 for the vaccination is similar to that shown in Figure 4A except that after the second vaccination, mice were sacrificed when the tumor volumes reached burden (2.0 cm^3). As expected, the average tumor volume of the saline-treated group increased more rapidly compared to the adjuvant only (CpG) and the nanovaccine plus adjuvant group (peptide-conjugated nanoparticles (Peptide NPs+CpG) with a statistically-significant difference at days 20 and 24 (Figure 5A). Notably, the average tumor volume of the CpG only group rose significantly after day 20 in comparison to the Peptide NPs+CpG group. Statistical significance between the CpG and the Peptide NPs+CpG group was observed at day 24 suggesting the latter was more potent at slowing tumor growth. Indeed, the Peptide NPs +CpG group had a median survival of 32 days compared to the CpG-treated cohort (26 days) (Figure 5B). There was no statistical significance in survival between the saline control group and the CpG only group, whereas statistical significance was observed between the Peptide NPs+CpG group (32 days) and the saline control group (20 days). No significant changes were observed in the weight of the mice (Fig. S14). The results indicate the effectiveness of the treatment with the nanovaccine in combination with the adjuvant.

In conclusion, we have demonstrated a generic approach for the preparation of biodegradable unimicellar nanovaccines based on hyperstar macromolecular chimeras with a capability of carrying multiple immunostimulating peptide antigens for cancer therapy as well as targeting peptides. Construction of a lipophilic branched core with high surface conjugation capacity akin of block copolymer micelles enabled the attachment of a large number of peptide antigens but low enough to circumvent entanglement between the peptides at a loading of 30 mol%, relative to available reactive surface groups. Saturation of the non-peptide conjugated reactive sites with a hydrophilic polymer, PEG_{12} mannose, gave core-shell like unimolecular micelles with a diameter of ca.20 nm based on DLS and 18 nm by TEM. The nanovaccines had good biocompatibility, and an evaluation of their efficacy in vivo as vaccines against B16 melanoma revealed increased T-cell accumulation in comparison to untreated mice. Moreover, mice treated with the nanovaccine and adjuvant (CpG) exhibited suppressed tumor growth and improved survival compared to non-treated and adjuvant-treated mice. We envisage that the incorporation of peptides targeted at reducing immune system evasion (e.g. TGF β) along with tumor peptide antigens is also

possible based on this strategy and may possibly enhance suppression of tumor growth.[33, 34] Overall, the demonstrated approach presents a promising strategy for the preparation multi-(neo)antigen bearing personalized nanovaccines and it is also highly adaptable towards the fabrication of nanostructures for imaging and diagnostic applications.

Supplementary Material

Refer to Web version on PubMed Central for supplementary material.

Acknowledgements

This work was financially supported by the National Institutes of Health (NIHR01CA112356, NIHR01CA199658, NIHR01CA211602, NIHR01CA210553, and NIHR01-CA134659).

The authors gratefully thank Dr. Steven George and Dr. Drew Elizabeth Glaser for their time, reagents and help in acquiring confocal microscopy images.

References

1. Luo M, Wang H, Wang Z, Cai H, Lu Z, Li Y, Du M, Huang G, Wang C, Chen X, Porembka MR, Lea J, Frankel AE, Fu Y-X, Chen ZJ and Gao J, Nat. Nanotech, 2017, 12, 648–654.
2. Zang X, Zhao X, Hu H, Qiao M, Deng Y and Chen D, Eur. J. Pharm. Biopharm, 2017, 115, 243–256. [PubMed: 28323111]
3. Goldberg Michael S., Cell, 2015, 161, 201–204. [PubMed: 25860604]
4. Yoon HY, Selvan ST, Yang Y, Kim MJ, Yi DK, Kwon IC and Kim K, Biomaterials, 2018 597–607. [PubMed: 29576282]
5. Kuai R, Ochyl LJ, Bahjat KS, Schwendeman A and Moon JJ, Nat. Mater, 2016, 16, 489–496. [PubMed: 28024156]
6. Frey S, Castro A, Arsiwala A and Kane RS, Curr. Opin. Biotechnol, 2018, 52, 80–88. [PubMed: 29597075]
7. Lauster D, Glanz M, Bardua M, Ludwig K, Hellmund M, Hoffmann U, Hamann A, Böttcher C, Haag R, Hackenberger Christian PR and Herrmann A, Angew. Chem. Int. Ed, 2017, 56, 5931–5936.
8. Ott PA, Hu Z, Keskin DB, Shukla SA, Sun J, Bozym DJ, Zhang W, Luoma A, Giobbie-Hurder A, Peter L, Chen C, Olive O, Carter TA, Li S, Lieb DJ, Eisenhaure T, Gjini E, Stevens J, Lane WJ, Javeri I, Nellaiappan K, Salazar AM, Daley H, Seaman M, Buchbinder EI, Yoon CH, Harden M, Lennon N, Gabriel S, Rodig SJ, Barouch DH, Aster JC, Getz G, Wucherpfennig K, Neuberg D, Ritz J, Lander ES, Fritsch EF, Hacohen N and Wu CJ, Nature, 2017, 547, 217. [PubMed: 28678778]
9. Sahin U, Derhovanessian E, Miller M, Kloke B-P, Simon P, Löwer M, Bukur V, Tadmor AD, Luxemburger U, Schrörs B, Omokoko T, Vormehr M, Albrecht C, Paruzynski A, Kuhn AN, Buck J, Heesch S, Schreeb KH, Müller F, Ortseifer I, Vogler I, Godehardt E, Attig S, Rae R, Breitkreuz A, Tolliver C, Suchan M, Martic G, Hohberger A, Sorn P, Diekmann J, Ciesla J, Waksmann O, Brück A-K, Witt M, Zillgen M, Rothermel A, Kasemann B, Langer D, Bolte S, Diken M, Kreiter S, Nemecek R, Gebhardt C, Grabbe S, Höller C, Utikal J, Huber C, Loquai C and Türeci Ö, Nature, 2017, 547, 222–226. [PubMed: 28678784]
10. Kapadia CH, Perry JL, Tian S, Luft JC and DeSimone JM, J. Control. Release, 2015, 219, 167–180. [PubMed: 26432555]
11. Aldous AR and Dong JZ, Biorg. Med. Chem, 2018, 26, 2842–2849.
12. Zhang L.-x., Xie X.-x., Liu D.-q., Xu ZP and Liu R.-t., Biomaterials, 2018, 174, 54–66. [PubMed: 29778982]
13. Buhrman JD, Jordan KR, Munson DJ, Moore BL, Kappler JW and Slansky JE, J. Biol. Chem, 2013, 288, 33213–33225. [PubMed: 24106273]
14. Lohse SE and Murphy CJ, J. Am. Chem. Soc, 2012, 134, 15607–15620. [PubMed: 22934680]

15. Luo M, Samandi LZ, Wang Z, Chen ZJ and Gao J, J. Control. Release, 2017, 263, 200–210. [PubMed: 28336379]
16. Gomes A, Mohsen M and Bachmann M, Vaccines, 2017, 5, 6.
17. Kakwere H and Perrier S, J. Am. Chem. Soc, 2009, 131, 1889–1895. [PubMed: 19154112]
18. Hartlieb M, Floyd T, Cook AB, Sanchez-Cano C, Catrouillet S, Burns JA and Perrier S, Polym. Chem, 2017, 8, 2041–2054.
19. Fan X, Li Z and Loh XJ, Polym. Chem, 2016, 7, 5898–5919.
20. Zheng Y, Li S, Weng Z and Gao C, Chem. Soc. Rev, 2015, 44, 4091–4130. [PubMed: 25902871]
21. Hutchings L, Angew. Chem. Int. Ed, 2012, 51, 2543–2543.
22. Kakwere H, Ingham ES, Allen R, Mahakian LM, Tam SM, Zhang H, Silvestrini MT, Lewis JS and Ferrara KW, Bioconjugate Chem, 2017, 28, 2756–2771.
23. Gaucher G, Dufresne M-H, Sant VP, Kang N, Maysinger D and Leroux J-C, J. Control. Release, 2005, 109, 169–188. [PubMed: 16289422]
24. Glaffig M, Palitzsch B, Stergiou N, Schüll C, Straßburger D, Schmitt E, Frey H and Kunz H, Org. Biomol. Chem, 2015, 13, 10150–10154. [PubMed: 26299280]
25. Lowe AB, Hoyle CE and Bowman CN, J. Mater. Chem, 2010, 20, 4745–4750.
26. Dommerholt J, Rutjes FPJT and van Delft FL, Top. Curr. Chem, 2016, 374, 16.
27. Yan ZY, Wu YH, Du JF, Li GD, Wang SD, Cao WP, Zhou XM, Wu CJ, Zhang D, Jing XL, Li YF, Wang HF, Gao YF and Qi YM, Oncotarget, 2016, 7, 40437–40450. [PubMed: 27250027]
28. Xie J, Yang C, Liu Q, Li J, Liang R, Shen C, Zhang Y, Wang K, Liu L, Shezad K, Sullivan M, Xu Y, Shen G, Tao J, Zhu J and Zhang Z, Small, 2017, 13, 1701741–1701759.
29. Alexander J, del Guercio M-F, Maewal A, Qiao L, Fikes J, Chesnut RW, Paulson J, Bundle DR, DeFrees S and Sette A, J Immunol, 2000, 164, 1625–1633. [PubMed: 10640784]
30. Irvine DJ, Swartz MA and Szeto GL, Nat. Mater, 2013, 12, 978–990. [PubMed: 24150416]
31. Li C, Zhang X, Chen Q, Zhang J, Li W, Hu H, Zhao X, Qiao M and Chen D, ACS Appl. Mater. Interfaces, 2018, 10, 2874–2889. [PubMed: 29285934]
32. Tullett KM, Leal Rojas IM, Minoda Y, Tan PS, Zhang J-G, Smith C, Khanna R, Shortman K, Caminschi I, Lahoud MH and Radford KJ, JCI Insight, 2016, 1, 1–12.
33. Tauriello DVF, Palomo-Ponce S, Stork D, Berenguer-Llergo A, Badia-Ramentol J, Iglesias M, Sevillano M, Ibiza S, Cañellas A, Hernando-Momblona X, Byrom D, Matarin JA, Calon A, Rivas EI, Nebreda AR, Riera A, Attolini CS-O and Batlle E, Nature, 2018, 554, 538–543. [PubMed: 29443964]
34. Romero D, Nat. Rev. Clin. Oncol, 2018, 15, 201. [PubMed: 29508859]

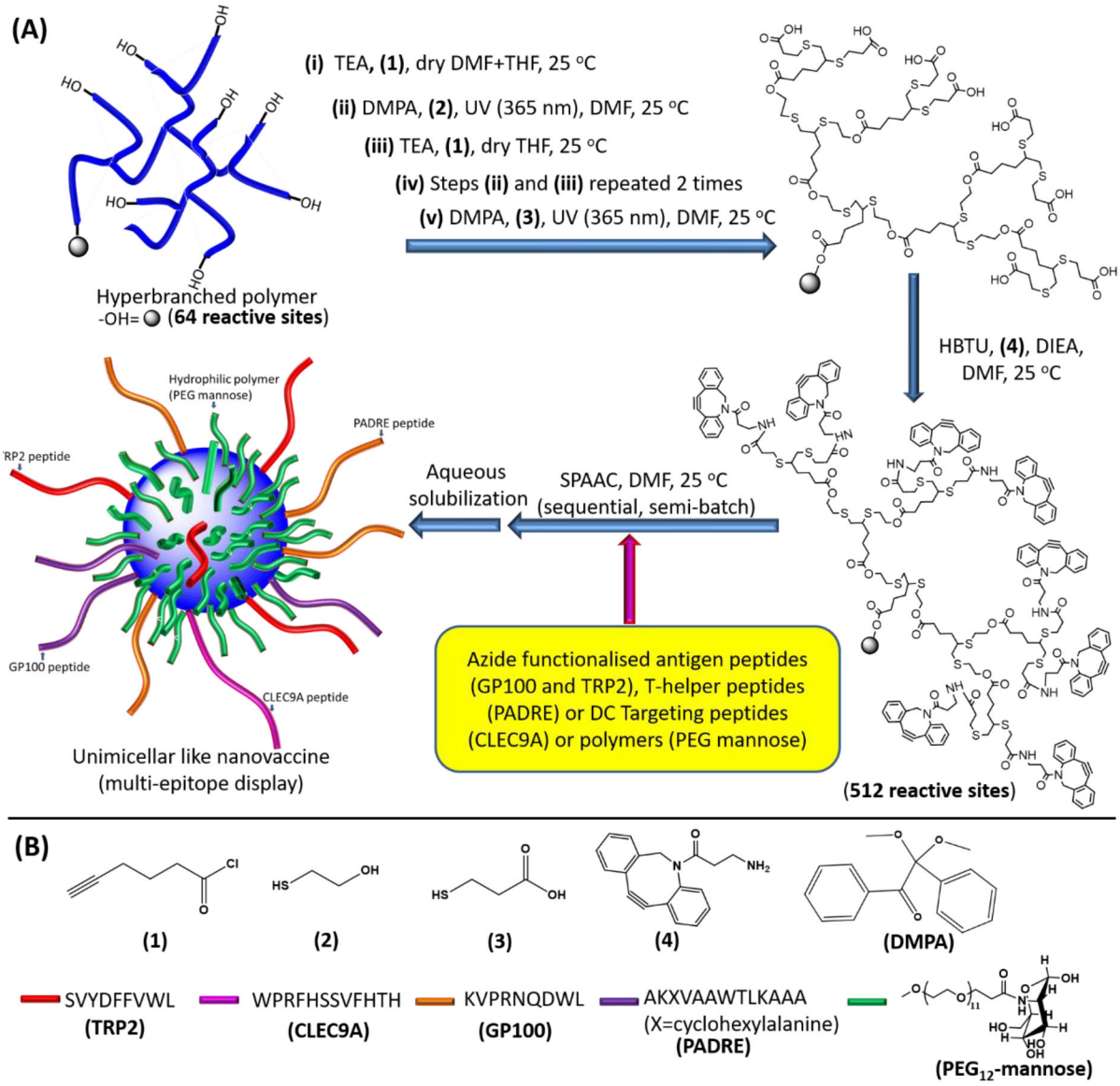

Fig. 1.

Approach followed for the preparation of unimicellar-like nanovaccines decorated with multiple peptide antigens, a T-helper peptide and a CLEC9A DC targeting peptide (A) and chemical structures of the reagents, peptide sequences and the PEG mannose polymer (B). *NB*: All peptides and PEG_{12} mannose are terminated with azide functionality (see ESI, Fig. S3–S6 for full structures for peptides and reference 22 for the structure of PEG_{12}−mannose).

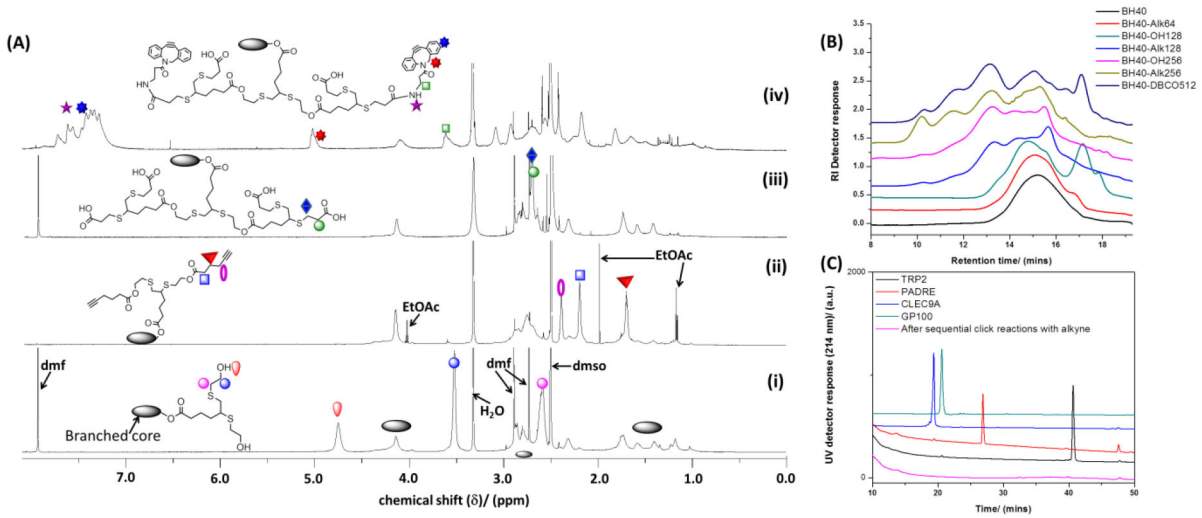

Fig. 2.

^{1}H NMR spectra of the lipophilic core construction (**A**), which was constructed from BH40 (64–OH groups), esterification of the–OH groups with (**1**) to BH40-Alk64, thiol-yne of BH40-Alk64 (64 alkyne groups) with (**2**) to BH40-OH128 (128–OH groups) and esterification of BH40-OH128 with (**3**) to BH40-Alk128 and repeat of the thiol-yne reaction with (**2**) etc. with BH40-Alk256 being terminated by (**4**) instead of (**2**). Representative spectra of repetitive thiol-yne click and esterification reactions (**i** and **ii**), (**i**) BH40-OH256 and (**ii**) BH40-Alk256, (**iii**) BH40-COOH512 (thiol-yne reaction between (**4**) and BH40-Alk256 (BH40 core with 256-alkyne groups)) and (**iv**) BH40-DBAC512 (from reaction between BH40-COOH512 and (**5**)). The SEC chromatograms for the construction of the core are shown in (**B**) (BH40-COOH512 does not elute). In (**C**), analysis of pure peptides and crude reaction mixture by HPLC after the strain-promoted azide-alkyne click (SPAAC) reaction of the alkyne core with azido peptides is shown.

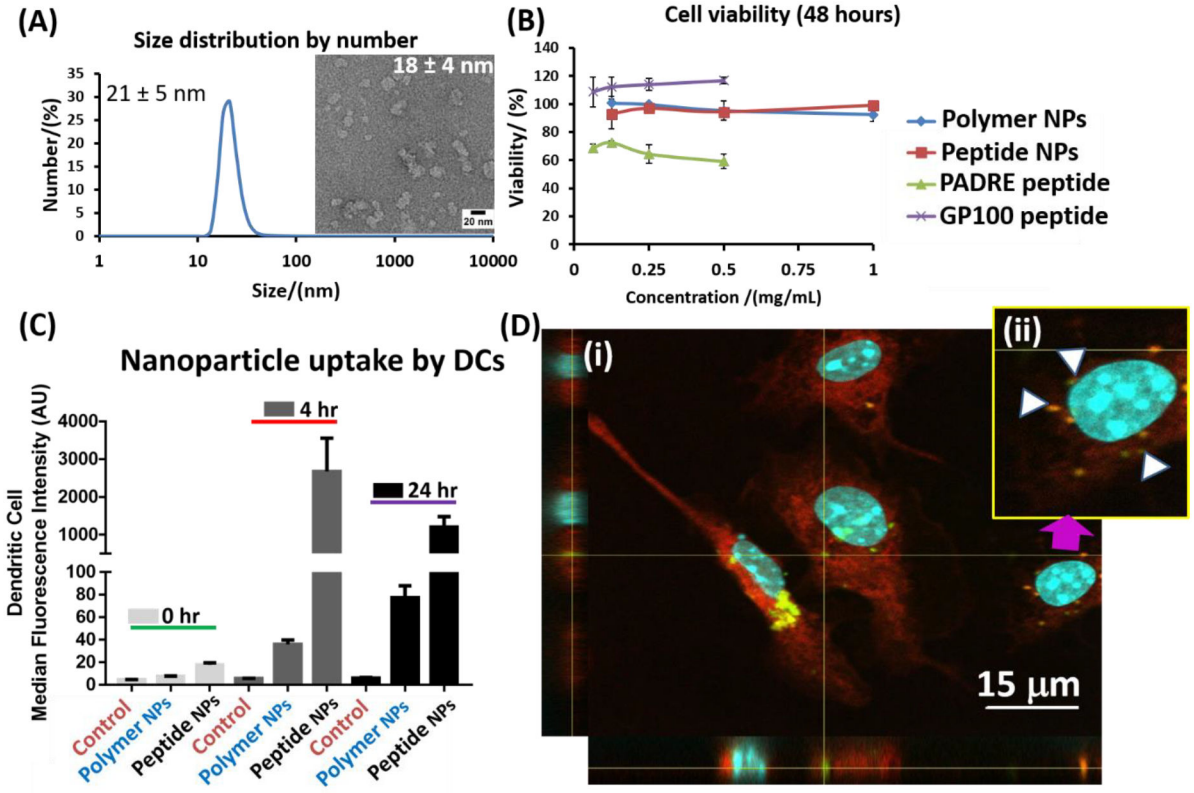

Fig. 3.

Size measurement of peptide-conjugated nanoparticles by DLS (average of 5 measurements) and an inset of the TEM image showing the morphology of the particles (scale bar = 20 nm) (**A**), cell viability of B16 melanoma cells incubated with polymer particles (Polymer NPs), peptides only and peptide-conjugated nanoparticles (Peptide NPs) at 37 °C for 48 hours (**B**) and internalization of fluorescein-labelled nanoparticles by DCs *via* flow cytometry (**C**) and, confocal microscopy images showing uptake of fluorescein-labelled peptide-conjugated nanoparticles by DCs in vitro after 4 hours of incubation at 37 °C. Co-localization of the LysoTracker stain (red) and fluorescein-labelled nanoparticles can be clearly observed (green spots pointed by white arrows in square showing an enlarged cell pointed by purple arrow (ii)). The nucleus appearing as bright light blue was stained by DAPI. More confocal images are available in ESI, Fig. S12.

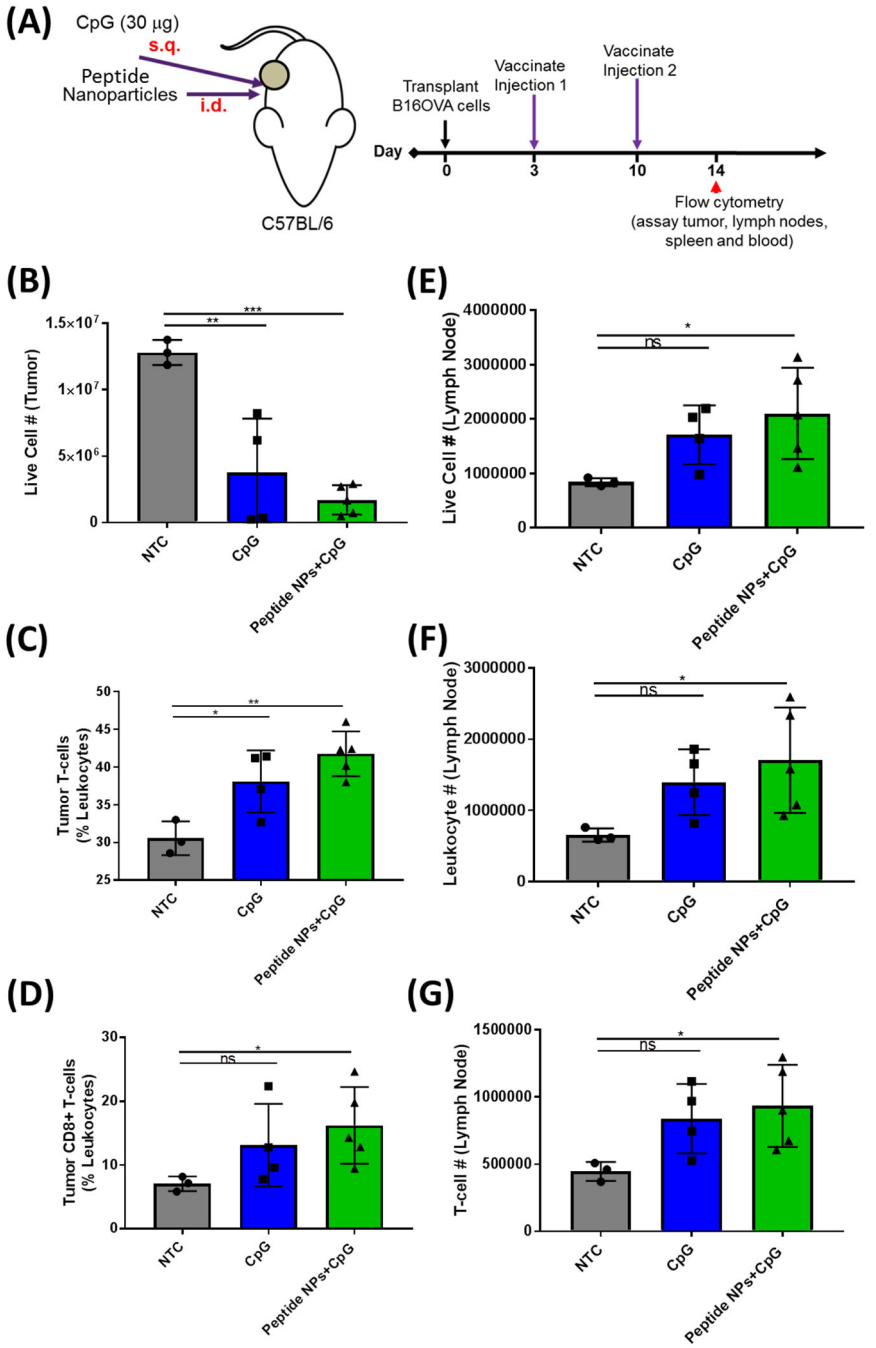

Fig. 4.

Vaccination protocol for the assessment of immune response *in vivo via* flow cytometry (NTC (*N*=3), CpG (*N*=4), Peptide NPs+CpG (*N*=5)), nanoparticles were administered intradermally while the adjuvant (CpG) was given *via* subcutaneous injection (A) and flow cytometry results of immune cell populations in the tumor and lymph nodes (B-G). For statistical significance, $p \leq 0.05$ (* $p \leq 0.05$, ** $p \leq 0.01$, *** $p \leq 0.001$).

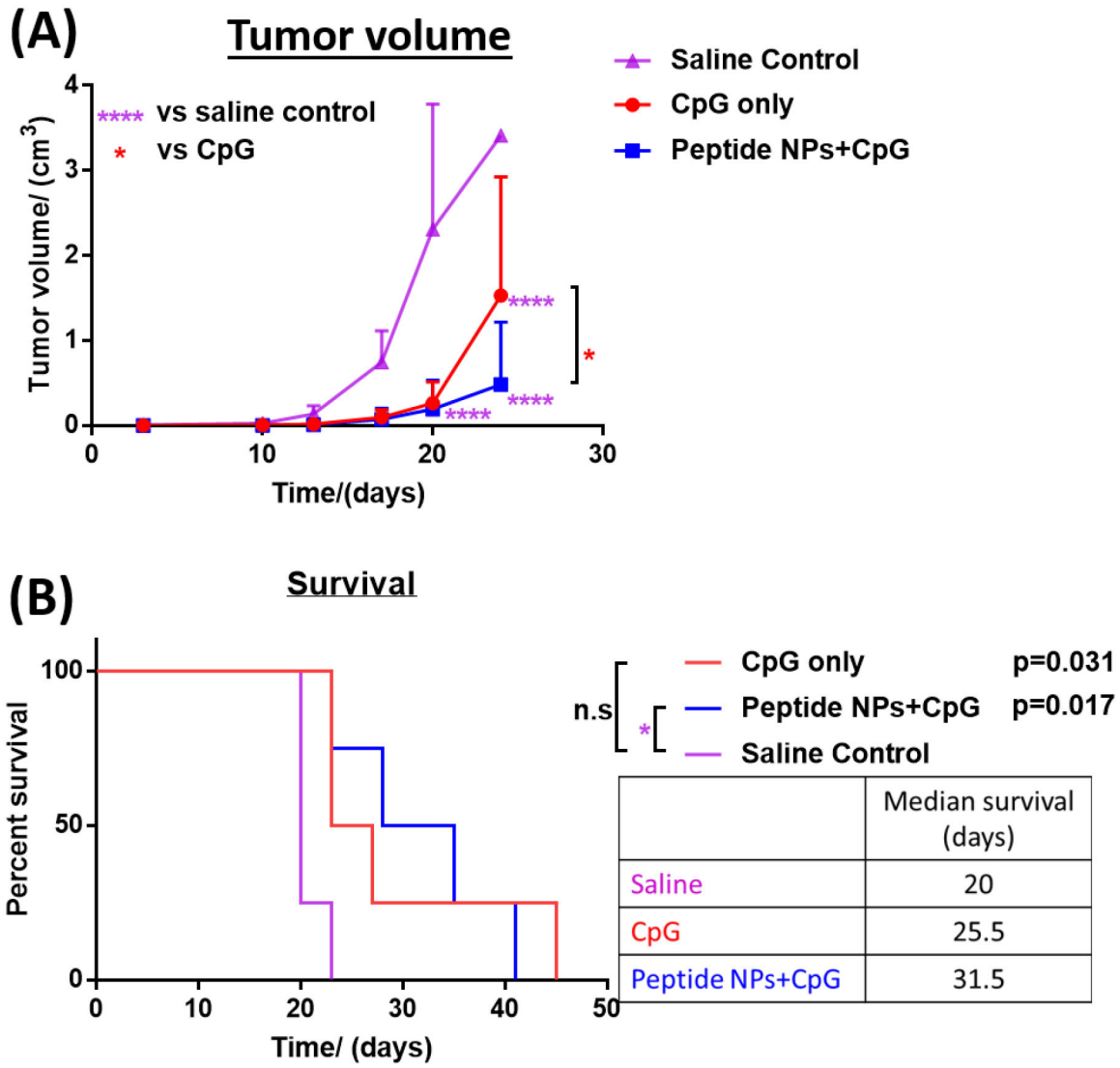

	Median survival (days)
Saline	20
CpG	25.5
Peptide NPs+CpG	31.5

Fig. 5.

Tumor volume (**A**) and survival study curves (**B**) of C57BL/6 mice implanted unilaterally with B16OVA tumor cells ((Saline, *N*=4), (CpG, *N*=4) and (Peptide NPs+CpG, *N*=4)). The vaccination procedure is similar to that shown in Fig. 4A. Significance for tumor growth (per time point) was assessed using ANOVA with a Tukey post-test with results being statistically significant when $p \leq 0.05$ (* $p \leq 0.05$, **** $p \leq 0.001$). For survival, results were considered to be statistically significant when $p \leq 0.017$ (Bonferroni corrected for three comparisons) (* $p \leq 0.017$). Animal weight curves are available in ESI, Fig. S14.